Title
COUPLED DIFFUSION OF CARBON ATOMS AND VACANCIES IN PLATINUM

Author
Ferguson, P.

Publication Date
1984-08-01

Lawrence Berkeley Laboratory
UNIVERSITY OF CALIFORNIA

Materials & Molecular Research Division

Submitted to Metals Science

COUPLED DIFFUSION OF CARBON ATOMS AND VACANCIES IN PLATINUM

P. Ferguson, K.H. Westmacott, R.M. Fisher and U. Dahmen

August 1984

Prepared for the U.S. Department of Energy under Contract DE-AC03-76SF00098

DISCLAIMER

Coupled Diffusion of Carbon Atoms and Vacancies in Platinum

P. Ferguson, K. H. Westmacott, R. M. Fisher and U. Dahmen

Materials and Molecular Research Division

Lawrence Berkeley Laboratory

University of California

Berkeley, CA 94720

Abstract

Direct evidence for the interstitial analogue of the reverse Kirkendall effect has been found in experiments of carbon diffusion through platinum membranes. The carbon diffusion was accompanied by the formation of protrusions and depressions in the carburized and decarburized surfaces respectively. The magnitude of the counterflux of platinum atoms suggests that a substantial fraction of the carbon atoms are strongly bound to vacancies. An analysis based on Lomer's equation yields a carbon atom-vacancy binding energy, $E^B_{v\text{-}c} \geq 0.5$eV.

Introduction

The occurrence of strong binding between interstitial carbon or nitrogen atoms and vacancies in Fe and other bcc metals is manifested in the recovery spectrum of irradiated alloys by a) the disappearance of the carbon or nitrogen internal friction peaks[1], b) retardation of carbide or nitride precipitation[2], and c) an increase of about 300°C in the vacancy migration temperature[3]. However, there is no direct evidence that the

association of carbon atoms and vacancies affects diffusion in unirradiated bcc metals. Recently, an electron microscopy study of precipitation in quenched Pt-C alloys[4,5] provided the first suggestion that coupled diffusion of tightly bound V-C pairs can occur in an fcc metal and prompted the present work. The experimental techniques employed stemmed from incidental observations of changes in surface structure of an Fe foil during studies of the catalytic gasification of bulk graphite[6]. In that work, the Fe foil was exposed to a carburizing atmosphere on one side and a decarburizing atmosphere on the other. The irregular appearance of the two surfaces suggested the possibility of a vacancy flux through the foil although the observations were not definitive. In a yet earlier study of carbon diffusion through austenite cylinders Smith[7] measured a nonlinear steady-state concentration profile but did not examine the surfaces. The present experiments were conducted to explore carbon diffusion through membranes in a simple system under more controlled conditions.

Experimental

Carbon diffusion experiments were performed using the arrangement shown schematically in Fig. 1. The sample was a 15mm diameter disc of platinum foil (0.1mm thick) mechanically polished to a 0.05μm finish on both surfaces. The material was from the same stock used in previous studies[4,5] and contained ~0.5at-% substitutional impurities (principally Rh, Pd and Ir) and $7.4 \pm 0.9 \times 10^{-2}$at-% carbon. A copper retaining ring secured the platinum disc on the top of the copper crucible that contained a commercial carburizing compound (10 wt-% Ba_2CO_3: 90 wt-% C) generating a carbon potential at temperature. After assembly, the crucible was suspended on a platinum wire and inserted into the cold (upper) end of a vertical tube furnace and supported there by attachment to a soft iron bob held by a magnet. The system was sealed, evacuated and filled with argon gas of 99.99% purity. Linear gas flow rates of 0.6cm s^{-1} were used and the gas pressure was maintained at slightly greater than atmospheric by 10-20mm of oil in an exit bubbler.

After about 2h the crucible was lowered into the furnace hot zone and after reaction the assembly was raised back into the cold portion of the furnace. Occasionally, a wet argon atmosphere was used and this was achieved by passing the argon through a water bubbler.

Heat-treated samples were examined in an ISI scanning electron microscope (SEM) operating at 25kV. Subsequently, 3mm discs were punched out for transmission electron microscopy (TEM) and electrochemically thinned from one side using the procedure outlined by Gath et al.[8]. The specimens were examined in a Siemens 102 and a Kratos 1.5MeV microscope operating at 100 and 900kV respectively. Auger spectra were recorded on a Physical Electronics Industries Model 590 scanning auger microscope (SAM). Samples were studied using a primary beam energy of 5keV and a primary beam current of 0.15μA.

Results

1. General Features

Characteristic features were observed on all samples subjected to carburizing/decarburizing treatments above about 600°C. The inner, carburized foil surfaces invariably showed extensive mounds of extruded material at the grain boundaries and to a lesser extent in the grain interiors. Conversely, on the outer, decarburized surfaces, extensive pitting, again enhanced in the grain boundaries, was observed. During the treatment the membrane also buckled away from the carburized side presumably due to the establishment of a pressure differential across the foil.

2. The Effect of Temperature

As expected, the phenomenon was found to be dependent on the reaction temperature. This is illustrated by the series of SEM micrographs given in Fig. 2. Images recorded with the beam normal to the carburized foil surface in the specimens treated at 700°C (a), 800°C (b), and 900°C (c) showed essentially similar amounts of extruded material at most of the grain boundaries while a progressive increase in the material deposited on

the grain interiors occurred with increasing temperature. It should be noted, however, that the reaction time was different in each case so that only a qualitative comparison is possible. In Fig. 2d the decarburized side of the 900°C treated sample is imaged in tilted illumination and the extensive pitting over the entire surface is clearly evident. Moreover, a comparison with the carburized side of the same foil (Fig. 2c) shows that a good correlation exists between the size and density of mounds on the inner surface and the pits on the outer surface. A further effect of increasing temperature is that both the mounds and pits become more hemispherical. A lower magnification micrograph of Fig. 2c given in Fig. 3 shows that whereas the size and distribution of mounds varies between different grain boundaries, it remains approximately constant within the grains. An alignment of the mounds and pits in the grain interiors is often evident. This is correlated with the presence of polishing scratches on the foil surfaces prior to the experiment.

3. The Effect of Decarburizing Atmosphere

Initial experiments were performed using commercial grade argon gas containing ~100ppm of water vapor. In subsequent experiments the water content was increased by bubbling the gas through water. A comparison of the results obtained at 800°C using the two different gas compositions is shown in Fig. 4. Fig. 4a, b, and c show respectively the decarburized (normal incidence), carburized (normal incidence) and carburized (tilted illumination) surfaces for the water-saturated argon treatment. Fig. 4d, e and f are the corresponding micrographs for the foils treated in the drier commercial gas. The significant differences evident may be attributed to less efficient decarburization in the drier gas. Thus, a comparison of the grain boundary regions in (a) and (d) indicates that a narrow, deep groove has formed in the wet gas atmosphere and a shallower, less pronounced groove bounded by regions which image differently from the matrix in the dry gas. Similarly, the (inner) carburized surface (b) is clear whereas that in (e) is decorated with a high density of particles which were analyzed to be rich in carbon. These observations suggest that the rate of reaction was limited by the rate of carbon diffusion

through the membrane in the wet argon but by the rate of removal of the carbon at the outer surface in the drier argon experiment. To test this hypothesis a detailed analysis was made of the surface region imaged in Fig. 4d. This specimen was back-thinned from the carburized side using the standard electropolishing technique. However, the resulting specimen had a very lacey appearance and examination in the TEM revealed the reason for this. The low magnification micrograph (Fig. 5a) shows that during electropolishing the regions adjacent to the grain boundaries were thinning at a significantly slower rate than the grain interiors. This in itself indicated the sample had a different composition near the grain boundaries, and confirmation was obtained from a subsequent Auger analysis of these regions. The same grain boundary was imaged after transferring the thinned sample to the SAM as seen in Fig. 5b (the images do not match exactly because an adjacent boundary strip was broken off during the transfer). The Auger spectrum recorded from this region (Fig. 6a) showed a very strong carbon peak at 240eV and a Pt peak at 1950eV which indicate a high carbon concentration in this region. A second spectrum recorded after sputtering 10nm of material from the surface with an argon beam (Fig. 6b) shows that the carbon is not on the surface. For comparison, a spectrum was taken from a grain interior (see Fig. 6c) and only Pt was detected. These results strongly indicate that a substantial enrichment of carbon has occurred in the regions adjacent to grain boundaries in the samples treated in the drier argon.

4. TEM Observations

To investigate further the microstructures resulting from the carburizing/decarburizing treatments, samples reacted in dry argon at 800°C were back-thinned to study the regions near the carburized and decarburized surfaces by TEM. The experiment is difficult to perform, because even pure platinum has a tendency to etch during thinning, thus the results must be analyzed with caution. Nevertheless, the observations were, in general, consistent with the SEM study.

An example of a foil taken from the carburized surface is shown in Fig. 7. Several distinctive features are evident. Dislocations are distributed in bands, A, and exhibit very strong, broad contrast indicating that they are heavily decorated with carbon. Dark circular spots, B, about 100nm in diameter are imaged particularly in the thinner regions of the foil. Their contrast and formation in rows suggest they are very small examples of the matrix surface mounds imaged in the SEM. Finally, a number of void-like features, C, are observed in association with the dislocation bands. This correlation suggests that they are not an artifact of the electropolishing; however, the possibility that they result from the preferential leaching of near-surface precipitates cannot be ruled out.

Fig. 8 shows a typical micrograph taken from the decarburized near-surface region. These structures all showed bands of void-like features, larger in size than on the carburized side, and many variations in matrix contrast indicative of a highly strained lattice. This latter feature is seen more clearly in Fig. 9a where severe foil buckling results in continuous bend contours throughout the specimen. Electron diffraction patterns taken from thin regions of this foil (Fig. 9b) showed superlattice reflections characteristic of an ordered phase, (presumably a carbide). The additional reflections appearing in the [100] zone and other patterns are consistent with a phase with twice the lattice parameter of the Pt matrix.

Discussion

The results clearly show that diffusion of carbon through the platinum foil, down the concentration gradient established by the carburizing/decarburizing boundary conditions, was accompanied by a flow of Pt atoms in the reverse direction. At 900°C, the highest annealing temperature used, normal self-diffusion would result in mass transport over distances of only ca. 2μm ($x \simeq 2\sqrt{Dt}$, where[9] $D = 10^{-13} cm^2 sec^{-1}$). This implies that the anomalously high Pt atom diffusion results from the counter flow of tightly-bound carbon atom/vacancy pairs diffusing as entities, as inferred from earlier quenching studies of Pt-C alloys.

It is interesting to compare and contrast this phenomenon with other examples of diffusion coupling solute atoms and point defects. In experiments of the Kirkendall type one substitutional atom species in a diffusion couple migrates more rapidly than the other leading to a counter flow of vacancies and the development of porosity on the side of the faster diffusing element. The vacancy flux in this case is induced by a solute atom concentration gradient. On the other hand, solute segregation can be induced in an initially homogeneous alloy by point defect gradients. In the case of vacancies diffusing to vacancy sinks, enrichment or depletion of the surrounding matrix can occur depending on whether solute atoms flow with or against the vacancy flux. The present example of Pt-C differs from both the Kirkendall effect and solute segregation in that (1) the diffusing solute atom is interstitial but nonetheless diffuses with a vacancy (2) the porosity forms on the exit surface, and (3) this reverse Kirkendall effect is induced by a solute rather than a vacancy gradient.

To test the concept of carbon driven vacancy diffusion, an estimate of the resulting vacancy flux was made using simplifying assumptions and an elementary model. The observations show that the mass transport is enhanced in grain boundary regions, and that dislocations in the matrix may also affect the diffusion process, but the case for a perfect lattice is considered first. It is assumed that the carbon concentration at the foil surface exposed to the carburizing atmosphere is maintained at its equilibrium value for the annealing temperature and that its value at the surface in contact with the decarburizing gas is zero. If carbon atoms are strongly bound to vacancies, the gradient in carbon concentration will give rise to a corresponding gradient in carbon atom-vacancy pairs, C_p. The concentration of pairs at the inner surface is given by Lomer's equation modified for the case of an interstitial impurity, i.e.

$$C_p = \exp(S_v^F/k)\exp(-E_v^F/kT)[6C_c \exp(E_{v-c}^b/kT)]$$

where the term outside the square brackets is the equilibrium vacancy concentration in pure platinum at temperature T, C_c is the equilibrium carbon concentration in the foil at T, and E^b_{v-c} is the vacancy-carbon atom binding energy. At the outer surface C_p is taken as zero. We now solve the diffusion equation to find the total vacancy and Pt atom fluxes deposited at the outer and inner surfaces respectively.

At 900°C both the vacancy pits and mounds have regular, readily measurable hemispherical shapes so the calculations will be compared with these data.

Taking $S^F_v/k = 0.35$,[10] $E^F_v = 1.3$eV[10] and T = 1173K, Eq. (1) reduces to

$$C_p = 2.2 \times 10^{-5}\, C_c \exp(9.91\, E^b_{v-c}) \ .$$

The appropriate values for C_c are not well known and the two reported values, 5×10^{-3} and 3.3×10^{-4}, differ by more than an order of magnitude[11,12]. The same is true of E^b_{v-c}; few attempts have been made to calculate or measure vacancy-interstitial impurity atom binding energies. Beeler[13], using computer simulation methods, estimated E^b_{v-c} = 0.3eV for carbon in nickel and since it is unlikely that in any system E^b_{v-c} greatly exceeds 0.5eV, these two values were used in the present calculations. The computed values of C_p with this limited range of parameters are given in the third row of Table I.

TABLE I

Calculated total atom fluxes at 900°C

C_c	5×10^{-3}	5×10^{-3}	3.3×10^{-4}	3.3×10^{-4}
E^b_{v-c}	0.3	0.5	0.3	0.5
C_p	2.1×10^{-6}	1.5×10^{-5}	1.4×10^{-7}	1×10^{-6}
$J_v t$	4×10^{15}	3×10^{16}	3×10^{14}	2×10^{15}

Since decarburization of the outer surface of the foil maintains C_c and $C_p = 0$ under steady state conditions $dC_p/dx = C_p/x$ where x is the foil thickness and the vacancy flux, J_v ($= -J_{Pt}$) can be found from Fick's First Law, $J_v = \frac{D_{v-c}}{\Omega}(C_p/x)$ provided the V-C complex diffusivity D_{v-c} is known. Since no direct evidence is available to show whether vacancy migration is perturbed by the presence of a tightly bound carbon atom, D_v for a monovacancy in Pt is used to estimate J_v. Taking $D_v = \gamma\nu a^2 \exp(S_v^m/k) \exp(-E_v^m/kT)$ with $\gamma = 1/12$, $\nu = 10^{13} s^{-1}$, $a^2 = 1.54 \times 10^{-15} cm^2$, $S_v^m/k = 1.2$, $E_v^m = 1.37eV$,[10] $x = 10^{-2}cm$, $\Omega = 15 \times 10^{-24} cm^3$, and $t = 16h$, the values of $J_v t$ given in Table I were obtained.

From Fig. 2c, $\bar{d}$, the average mound diameter, was estimated to be 10^{-4}cm, and n, the areal density, $3.6 \times 10^7 cm^{-2}$. Substitution of these values in the expression for the total atom flux that formed the mounds, i.e. $J_{Pt}t = \pi n \bar{d}^3/12$ yielded a value of 6×10^{17} atoms cm^{-2}. A comparison of the grain boundary and matrix mound sizes was made to estimate the ratio of mass transport in the boundaries and matrix. Although a variation in the mound size and spacing is seen in different boundaries (see Figs. 2 and 3), the size seems to be proportional to the spacing suggesting that the total flux is approximately constant. Using $\bar{d}_{gb} = 4 \times 10^{-4}$cm and the mean separation, $\bar{\ell} = 6 \times 10^{-4}$cm from the largest mounds seen in Fig. 2c and a mean grain size of 5×10^{-3}cm, the total atom flux traversing the boundary regions was found to be also ~8×10^{17} atoms cm^{-2}. The bulk flux is seen to be an order of magnitude larger than the estimate obtained using the higher values for C_c and E_{v-c}^b. In view of the assumptions made and the uncertainty in the parameters used in the calculations, some discrepancy is not unexpected. Several factors not accounted for could lead to a better agreement. For example, the TEM observations show that the voids and carbon enrichment appear to be associated with the bands of dislocations running through the matrix. These dislocations even if they do not run entirely through the foil, will lead to short circuit diffusion of the complexes. Alternatively, the agreement can be made exact, of course, by increasing E_{v-c}^b to ~0.6eV.

The carbon-vacancy binding energy could also be calculated if the carbon flux were known. In principle the amount of carbon that passed through the Pt could be determined from before and after weight measurements of the carburizing compound. Because the weight losses due to leakage and spillage are relatively large, the measured values leading to C:V ratios varying between 1000:1 and 100:1 are not reliable (a closed system with a gas chromatograph could achieve the desired accuracy). However, an estimate based on these ratios again results in a binding energy of between 0.4 and 0.6eV.

The large carbon atom-vacancy binding energy may have its origin in size effects. In the hard sphere model, carbon dissolved interstitially in FCC metals is oversize by amounts ranging from 29% in Au to 51% in Ni (37% for Pt) and from simple reasoning, this would be expected to lead to strong attractive interactions with a vacancy strain field. By comparison, atomic misfits in substitutional alloys for which binding energies have been measured are usually less than ~15%. Recent studies of diffusion of hydrogen through aluminum membranes by Hashimoto et al.[14] provide further evidence for strong interstitial atom-vacancy binding. It was found that when the membrane was in contact with hydrogen gas at 1 atmosphere at 350-400°C, diffusion through the foil occurred by a vacancy mechanism. When the foil was electrochemically charged to higher hydrogen concentrations at room temperature, the observed diffusion coefficient was four orders of magnitude higher than that estimated from extrapolation of the 350-400°C temperature data. This was interpreted in terms of diffusion by the usual interstitial mechanism. An analysis of the higher temperature data using Lomer's equation yielded a value of ~0.6eV for the hydrogen/vacancy binding energy in good agreement with the present estimate for carbon in Pt.

These results provide convincing evidence that interstitial impurity atoms and vacancies can, in some circumstances, migrate as strongly bound pairs. However, hydrogen, interstitially dissolved in aluminum, is about as much undersized on the

octahedral sites as carbon in Pt is oversized (~37%), so unless both positive and negative misfit lead to strong binding to vacancies, other factors (e.g. electronic effects) must be considered.

A surprising implication of the present observations is that a vacancy-carbon atom complex diffuses as an entity not only through the lattice but also along dislocations and grain boundaries. In terms of the simple misfit concept discussed earlier, the vacancy would be expected to lose its identity on the dislocation by producing, or being absorbed on, jogs, and the freed carbon atom should migrate rapidly along the disordered regions of the dislocation core. Similarly, grain boundaries should provide easy paths for interstitial impurity atom diffusion.

A possible explanation of the anomalous behavior may be suggested on the basis of the TEM observations. It is clearly evident from the very strong contrast exhibited in Fig. 7 that all the dislocations are heavily decorated. If both the dislocations and grain boundaries become saturated with atmospheres of carbon atoms during the initial stages of the experiments, the subsequent diffusion of further carbon may still represent short-circuit diffusion but it may require an accompanying vacancy in the now far less disordered carbon-enriched environment.

The retention of significant amounts of carbon in the foil is also indicated by the Auger data and the electron diffraction evidence obtained from the outer surface regions. The appearance of superlattice spots half way between the fundamental Pt spots indicates the presence of an ordered phase with twice the lattice parameter of platinum. This phase appears to be the same as that identified by electron diffraction from foils prepared by co-depositing layers of platinum and carbon and heating to 1100°C, as reported by Hansen[15]. Similar patterns have also been obtained recently from regions adjacent to large undissolved carbide particles in platinum[16]. Other observations reported in the literature also support this picture. For example, in preliminary diffusion experiments by Selman et al.[12], high purity graphite was sealed under vacuum in Pt tubing and annealed

in air at 1400°C. After 100 h the outer surfaces of the tube were severely distorted and the grain boundaries had opened up. These effects were attributed to the rapid diffusion of carbon through the walls and combustion at the outer surface. What appears to be a related effect was reported by Mykura[17]. In this study the usual grain boundary grooving was found in pure nickel heated in vacuo to 1000-1200°C; however, ridges of extruded material were observed at the boundaries in impure nickel. It was proposed that gas bubbles nucleated from carbon and oxygen impurities in the nickel and grew by absorbing vacancies transported from the surfaces down the grain boundaries.

In conclusion, if large interstitial solute-vacancy binding energies are common in both fcc and bcc metals, interesting consequences are implied. For example, extreme cases of solute atom segregation to grain boundaries and other vacancy sinks might be predicted. In most bcc metals, the majority of vacancies would be associated with residual impurity atoms at all but high temperatures, thus affecting diffusion and precipitation behavior. A marked dependence of radiation damage structure on interstitial content would also be expected.

Further more refined experiments to confirm the large binding energy values are planned for other alloy systems.

Summary and Conclusions

The observation of mounds on the inner surfaces and pitting on the outer surfaces of Pt foils subjected to carburizing/decarburizing treatments is attributed to a strong vacancy-carbon atom binding energy leading to a reverse Kirkendall effect.

Enhancement of the effect at grain boundaries is consistent with short-circuit diffusion along the boundaries.

A comparison of the magnitude of the effects with a simple analysis based on Lomer's equation shows good agreement and yields a value for the vacancy-carbon atom binding energy of ~0.5eV. Thus, paradoxically, impurity-vacancy binding energies appear

to be much larger in some interstitial alloys than in their much more studied substitutional counterparts.

Acknowledgements

This work is supported by the Director, Office of Energy Research, Office of Basic Energy Sciences, Materials Sciences Division of the U. S. Department of Energy under Contract No. DE-AC03-76SF00098.

References

1. H. Wagenblast and A. C. Damask, J. Phys. Chem. Solids 23, 21 (1961).
2. H. Wagenblast, F. E. Fujita and A. C. Damask, Acta Met. 12, 347 (1964).
3. B. Nielsen, A. Van Veen, L. M. Caspers, H. Filius, H. E. Hansen and K. Petersen in "Positron Annihilation", P. G. Coleman, S. C. Sharma and L. M. Diana (eds.), North Holland (1982), p. 111.
4. K. H. Westmacott and M. I. Perez, J. Nucl. Mat. 83, 231 (1979).
5. M. J. Witcomb, U. Dahmen and K. H. Westmacott, Acta Met. 31, 743 (1983).
6. A. Szirmae, V. U. S. Rao and R. M. Fisher, Proc. 9th Int. Cong. Electron Microscopy, Toronto (1978), Vol. 1, p. 452.
7. R. P. Smith, Acta Met. 1, 578 (1953).
8. J. B. Gath, A. S. Darling and E. F. I. Roberts, Prakt. Metallog. 6, 228 (1969).
9. G. Rein, H. Mehrer and K. Maier, phys. stat. sol. (a) 45, 253 (1978).
10. W. Schüle and R. Scholz, phys. stat. sol. (b) 93, K119 (1979).
11. R. H. Siller, W. A. Oates and R. B. McLellan, J. Less-Comm. Metals 16, 71 (1968).
12. G. L. Selman, P. J. Ellison and A. S. Darling, Platinum Met. Rev. 14, 14 (1970).
13. J. R. Beeler, Jr., Interatomic Potentials and Simulation of Lattice Defects", Plenum Press , N. Y. (1972), 339.

14. E. Hashimoto, K. Ono, Y. Murakami and T. Kino, "Point Defects and Defect Interactions in Metals", Univ. of Tokyo Press (1982), p. 496.

15. M. Hansen, "Constitution of Binary Alloys", McGraw Hill, N. Y. (1958), p. 377.

16. M. J. Witcomb, K. H. Westmacott and U. Dahmen, to be published.

17. H. Mykura, Phil. Mag. 4, 907 (1959).

Figure Captions

Fig. 1. Schematic of copper crucible used in carbon diffusion experiments.

Fig. 2. SEM micrographs of inner surface of platinum foil carburized at 700°C (a) 800°C (b) and 900°C (c) showing mounds of extruded material. The outer, decarburized, foil surfaces exhibit pitting as seen in (d) for the 900°C heat treatment.

Fig. 3. Low magnification view of area shown in Fig. 2c illustrating the distribution of mounds in the grain interior and grain boundaries of inner foil surface carburized at 900°C.

Fig. 4. Comparison of foil surfaces obtained by heat treatment at 800°C in water-saturated argon (left column a,b,c) and nominally dry argon (right column d,e,f).

Fig. 5. (a) TEM micrograph of same sample as shown in Fig. 4d back-thinned from the carburized side with grain interiors etched out. (b) The same area seen tilted in a SAM where an Auger spectrum of boundary area was recorded.

Fig. 6. Auger spectra showing enrichment of carbon in grain boundary regions. (a) probe positioned on grain boundary region indicated in Fig. 5. (b) same area after removing 10nm of the surface by sputtering. (c) spectrum from grain interior.

Fig. 7. TEM micrograph of carburized inner foil surface after 800°C heat treatment in dry argon. Typical features are dislocation bands (A), circular mounds or precipitates (B), and holes or voids (C).

Fig. 8. TEM micrograph of decarburized outer foil surface after 800°C heat treatment in dry argon. Note bands of voids or holes.

Fig. 9. TEM micrograph (a) and selected area diffraction pattern (b) of same foil as in Fig. 8. Bend contours indicate highly strained lattice. Note diffuse intensity in SAD.

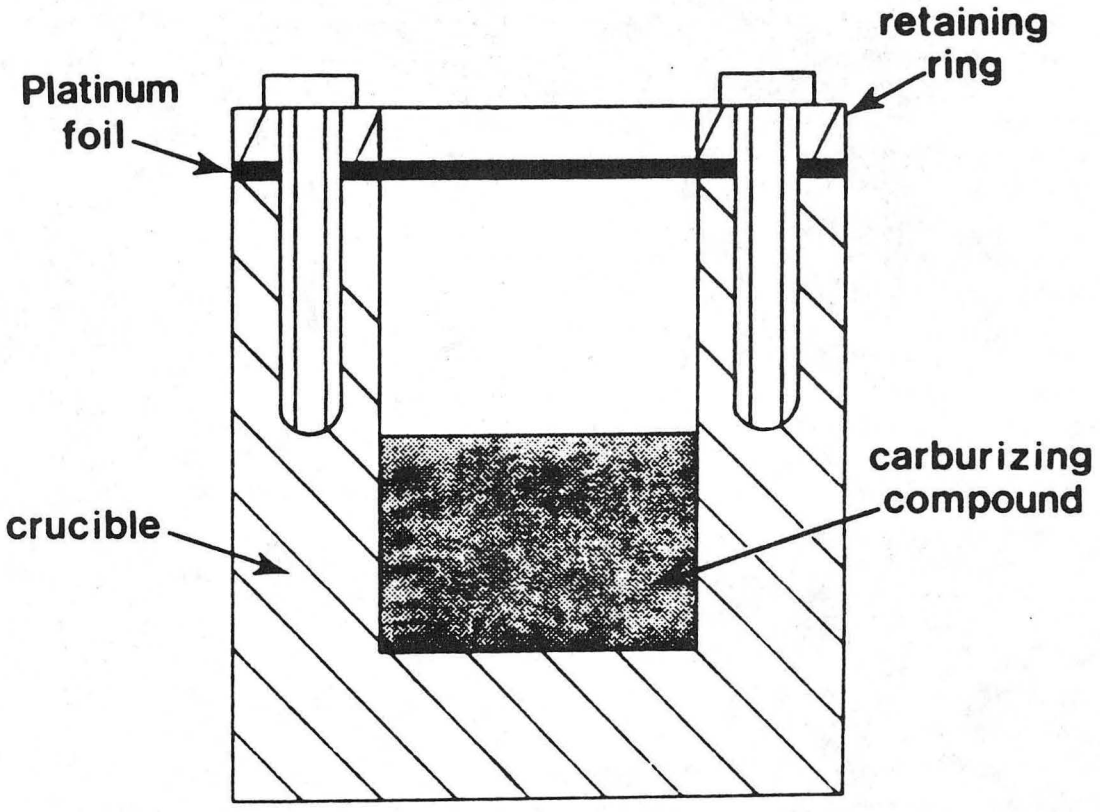
retaining
ring
Platinum
foil
carburizing
compound
crucible
XBL 844-1454

Fig. 1

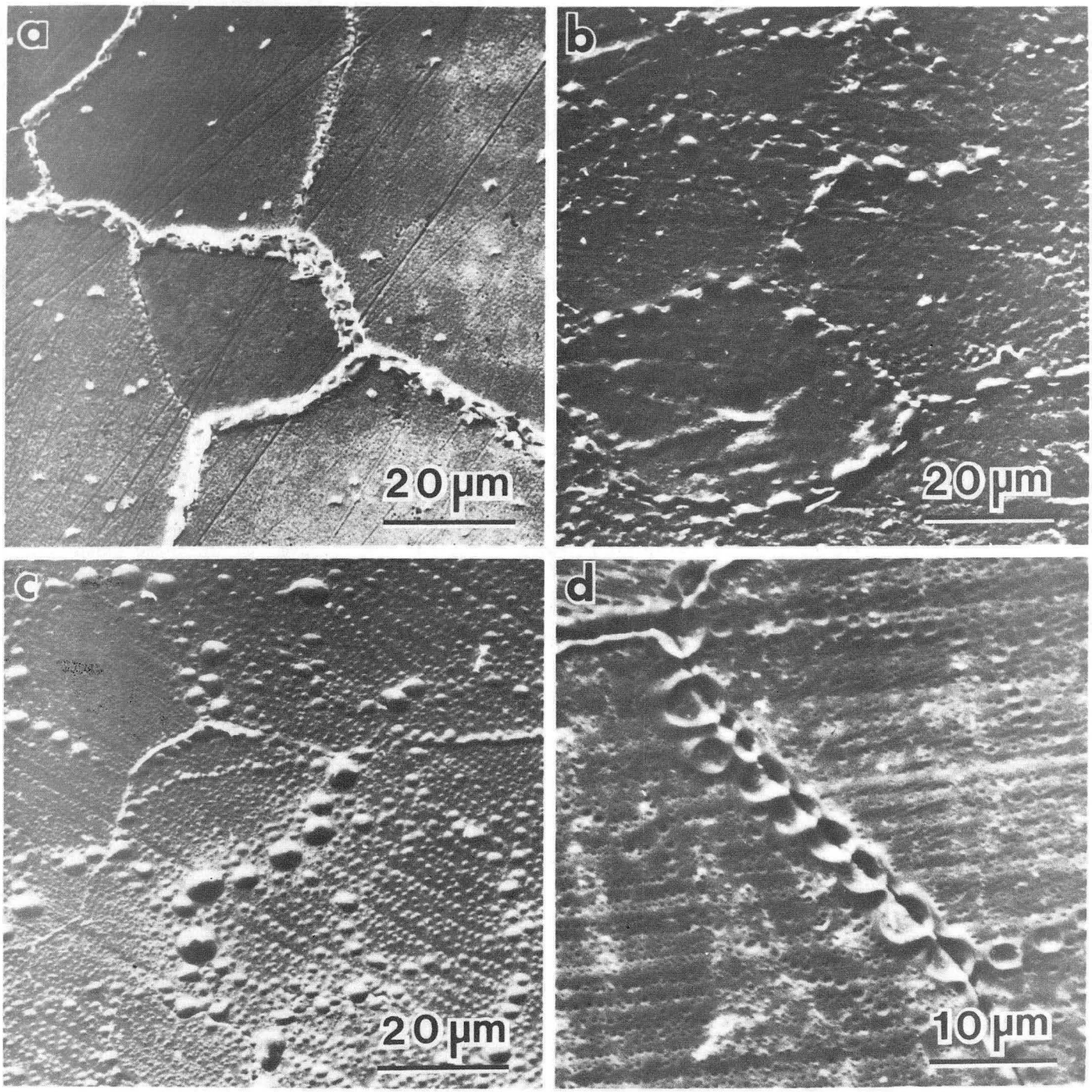

XBB 844-2820

Fig. 2

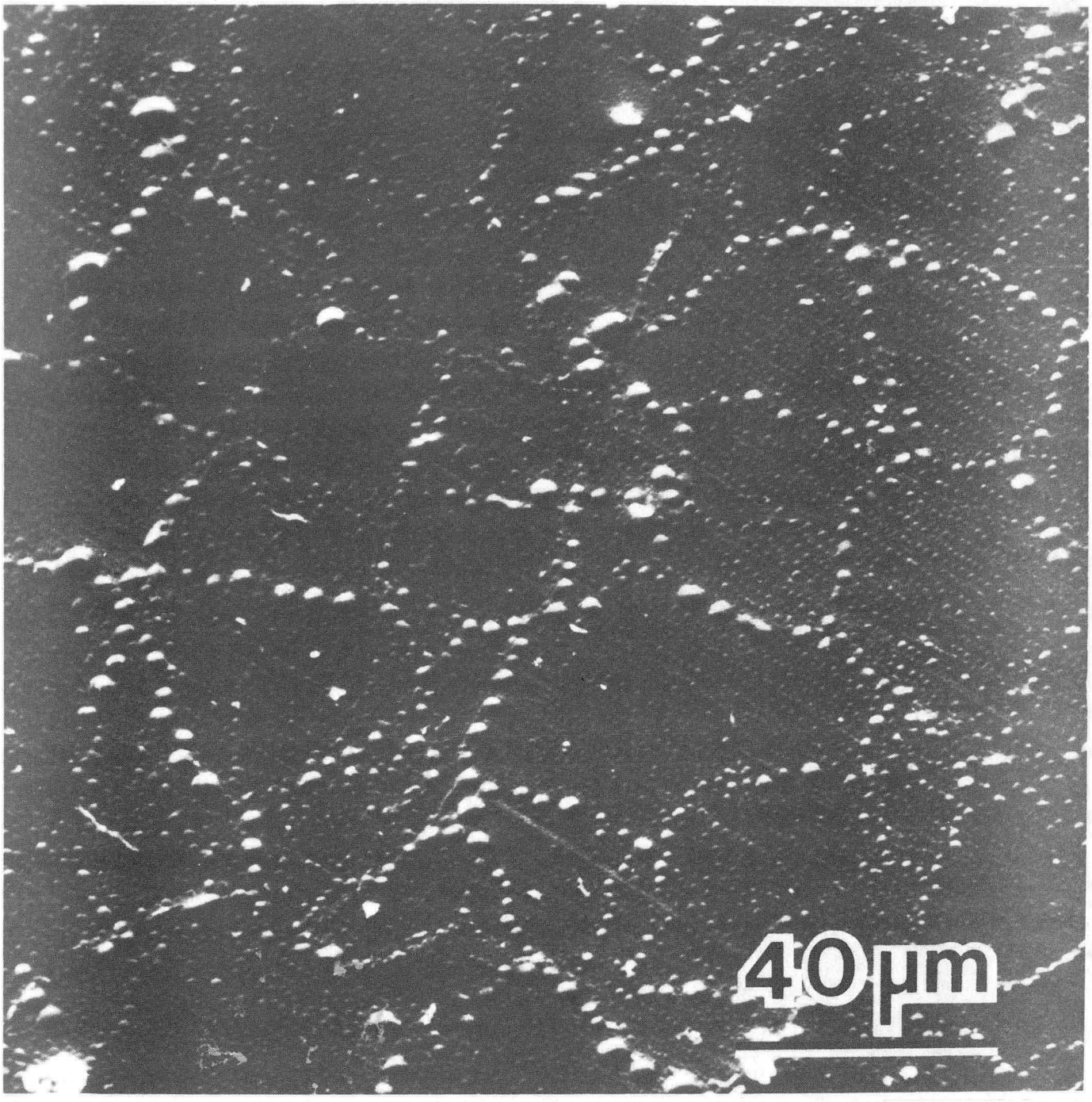

XBB 844-2819

Fig. 3

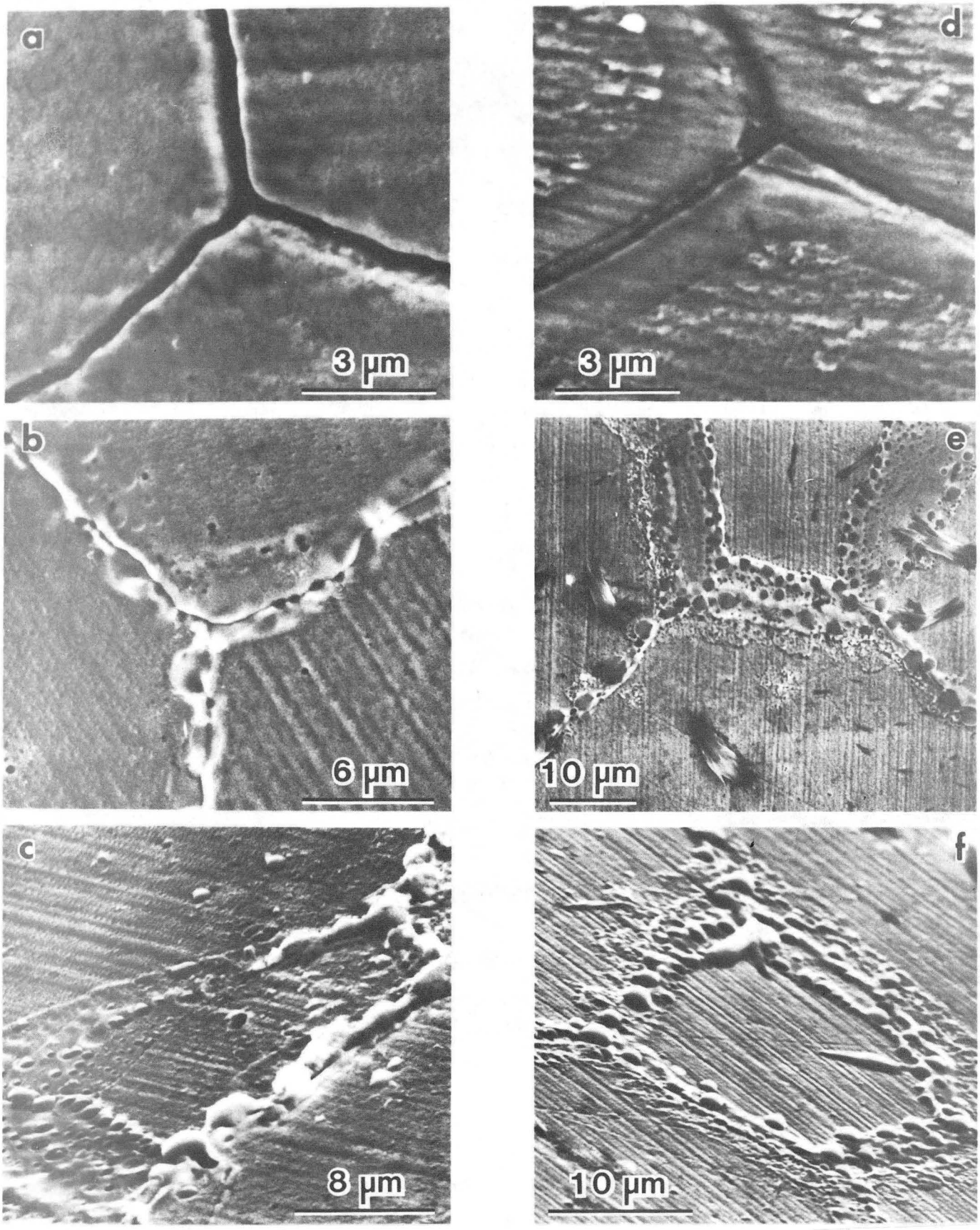

XBB 844-2705

Fig. 4

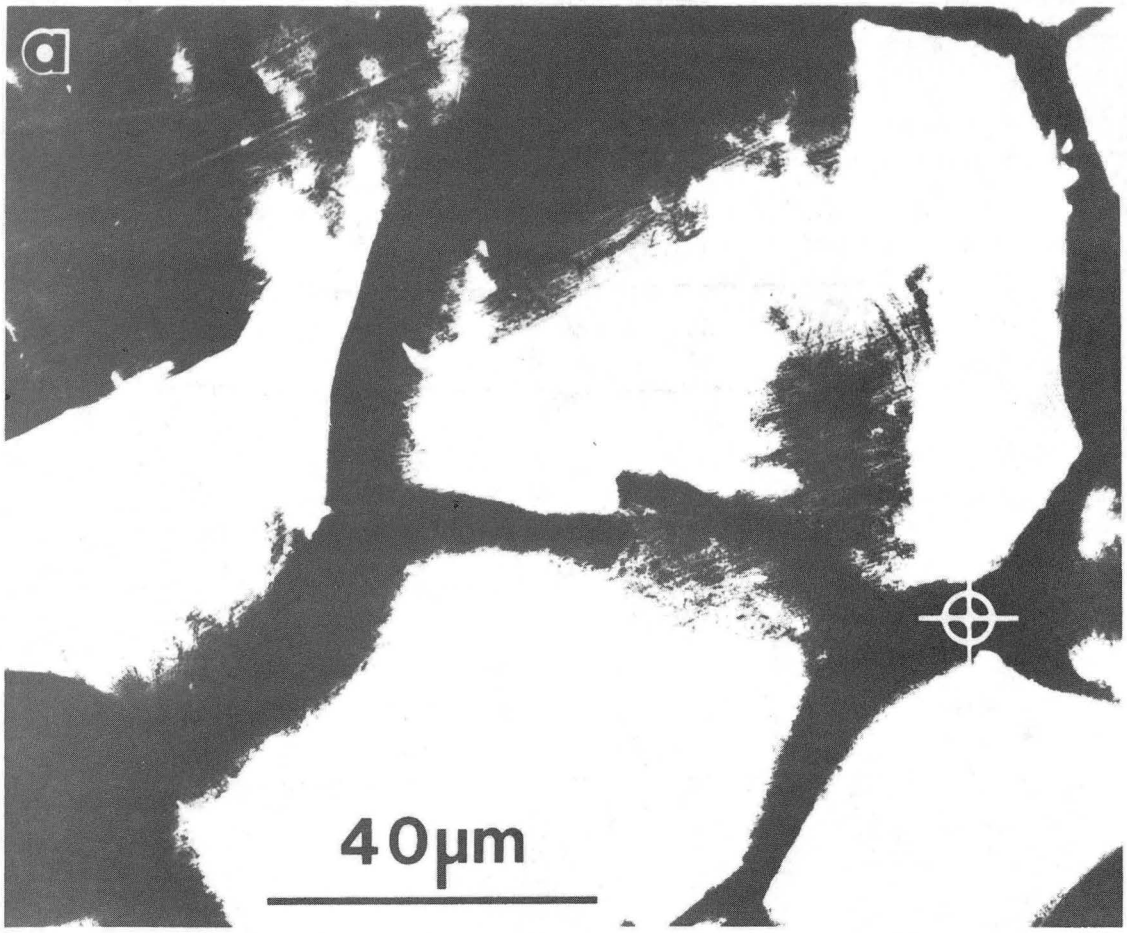

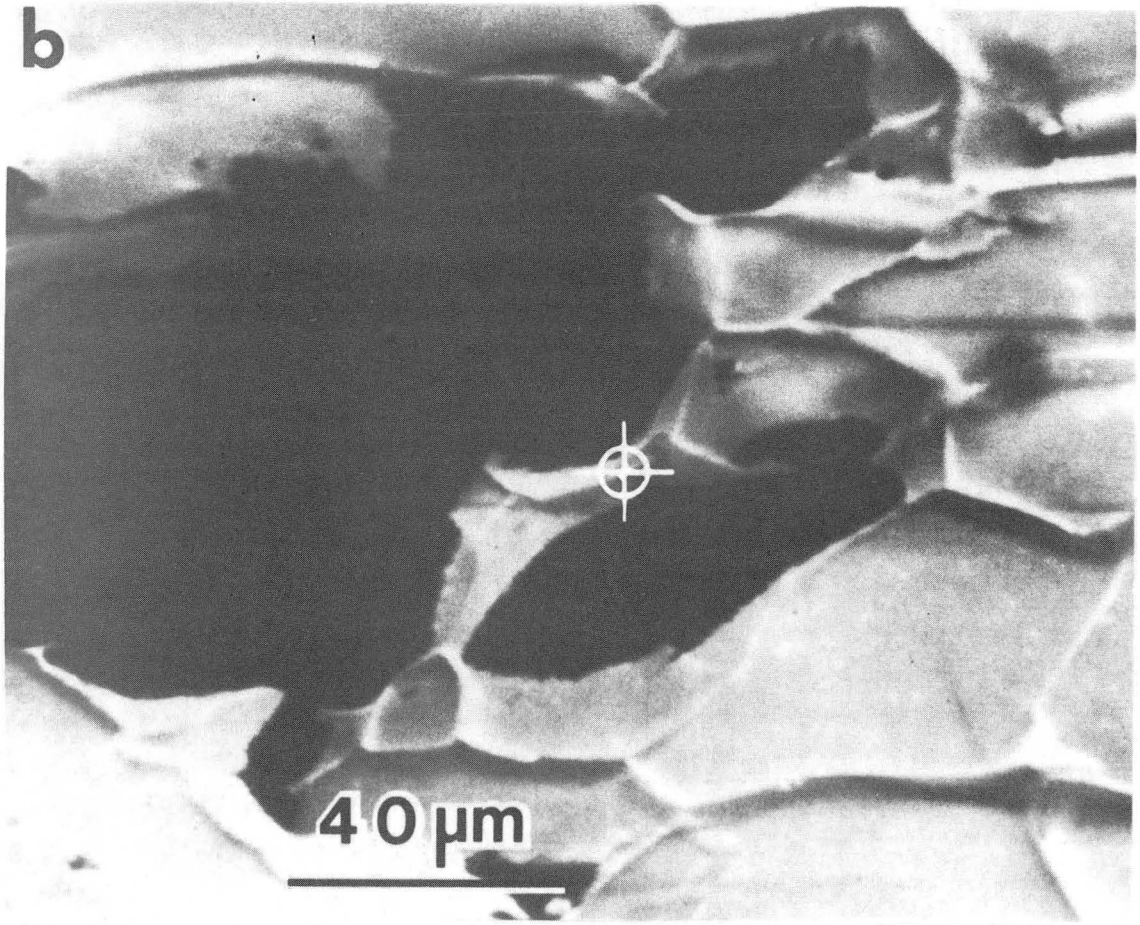

Fig. 5

XBB 844-2703

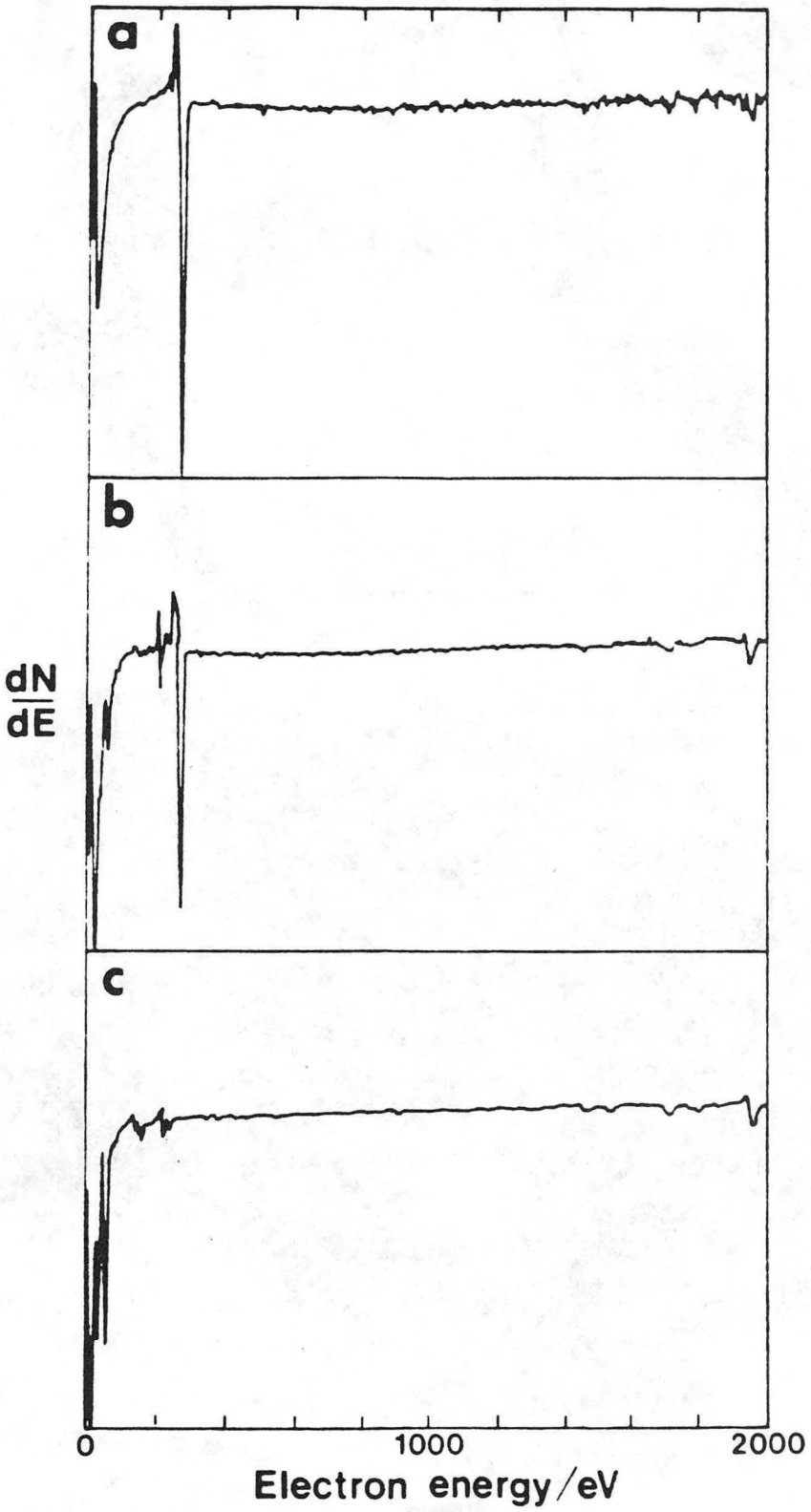

Fig. 6

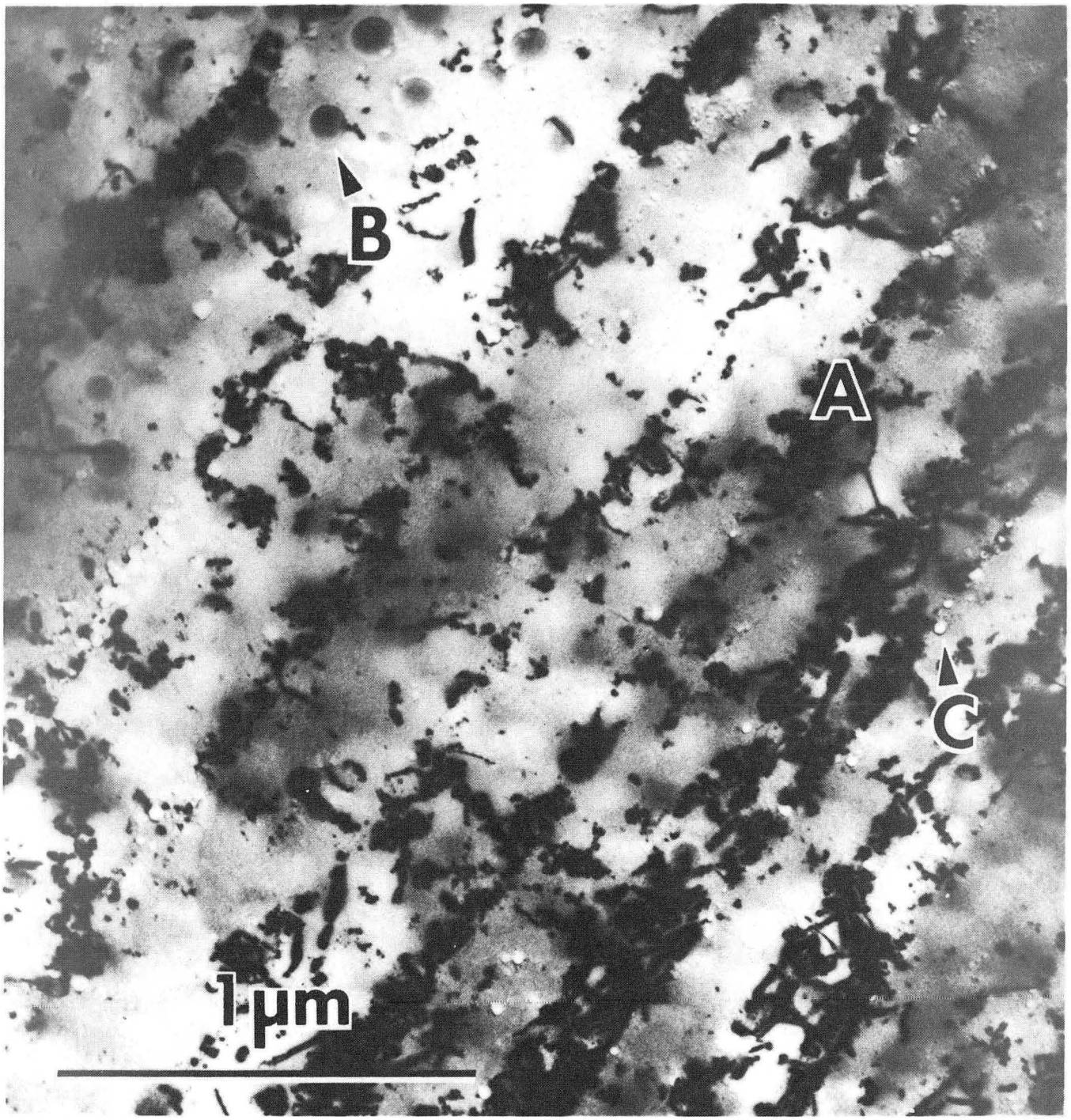

XBB 844-2701

Fig. 7

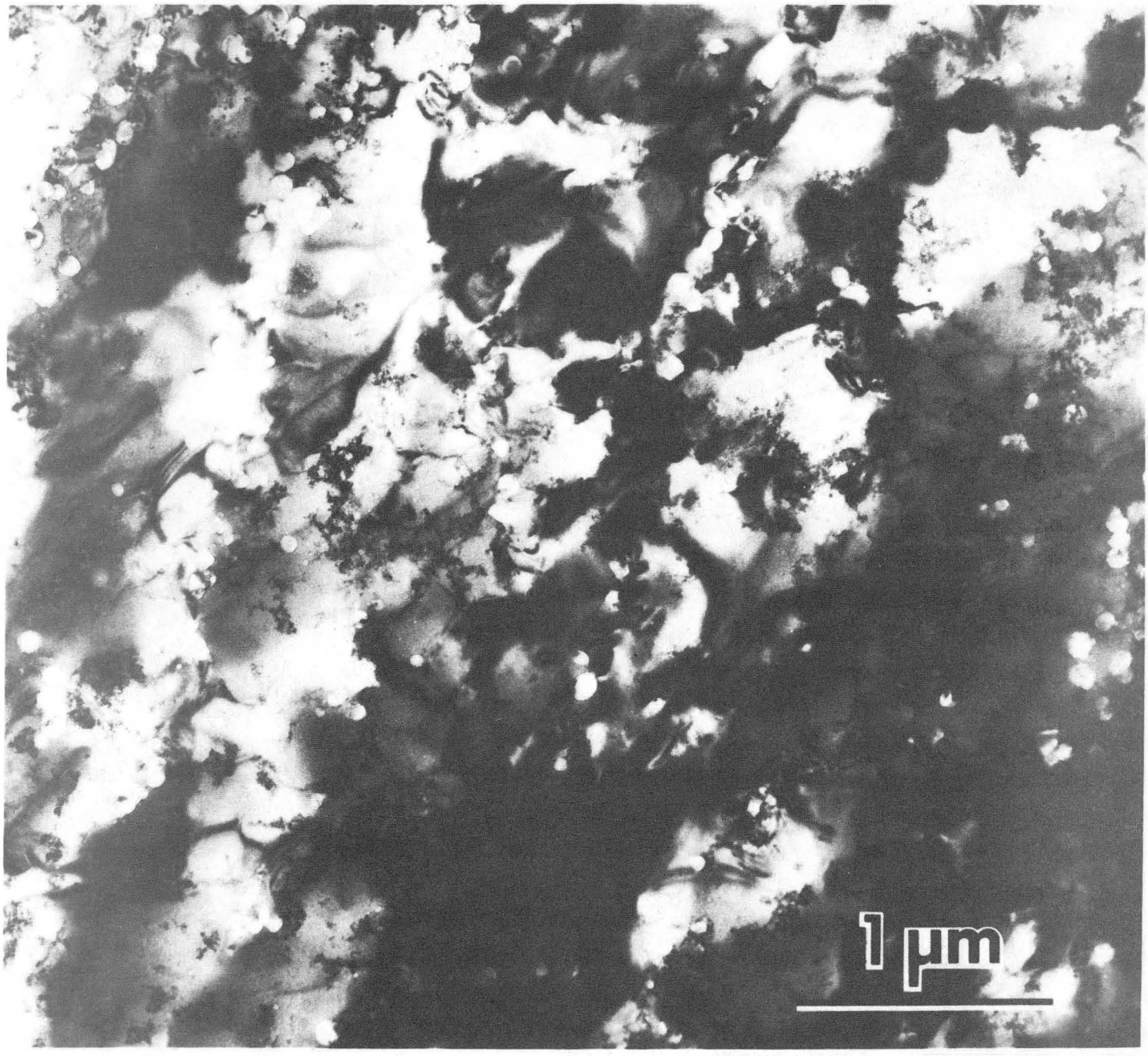

XBB 844-2702

Fig. 8

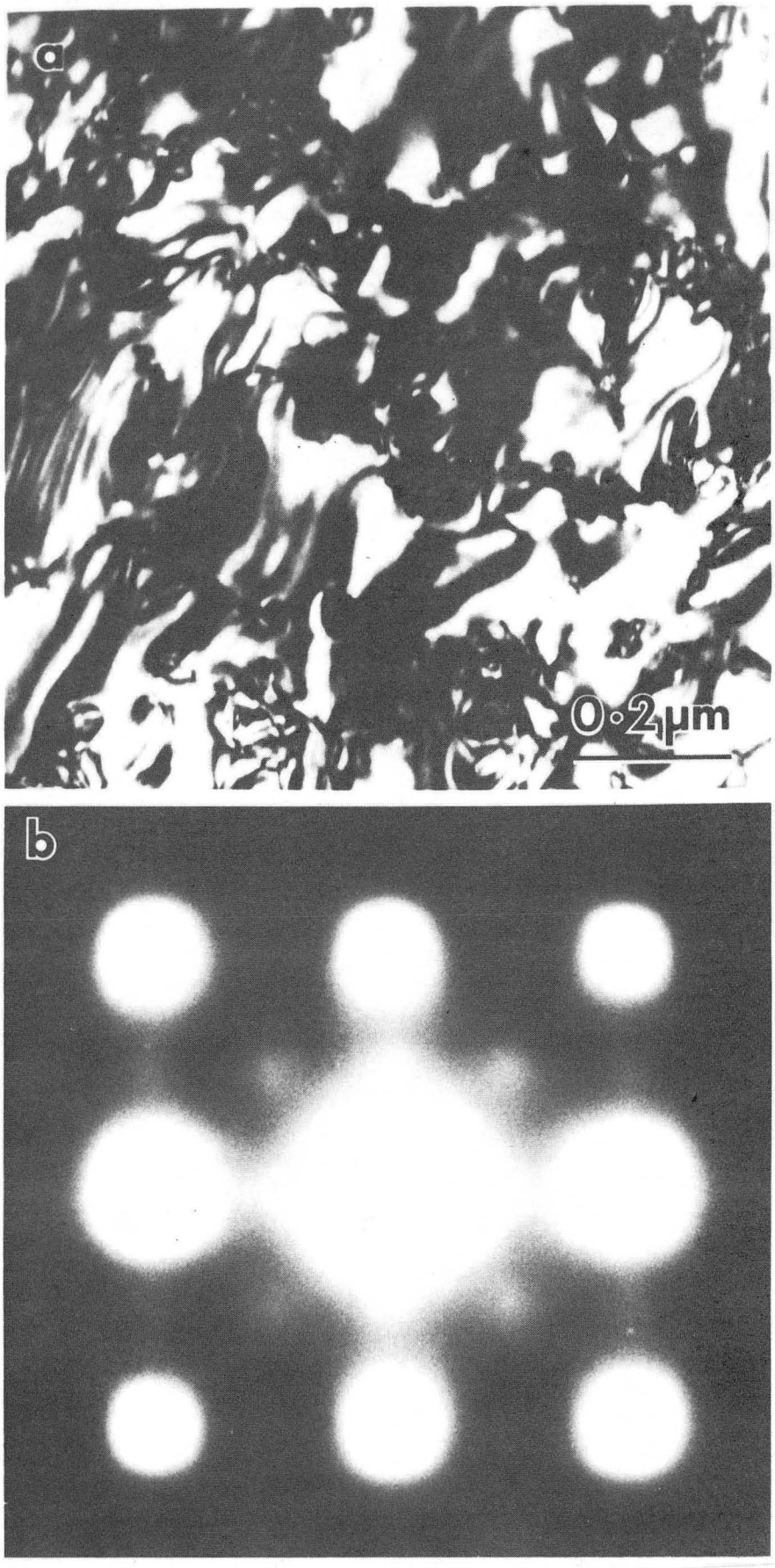

XBB 844-2704

Fig. 9

TECHNICAL INFORMATION DEPARTMENT
LAWRENCE BERKELEY LABORATORY
UNIVERSITY OF CALIFORNIA
BERKELEY, CALIFORNIA 94720